Hybrid Silica Cage-Type Nanostructures Made from Triply Hydrophilic Block Copolymers Single Micelles

Anu Vashishtha, Anthony Phimphachanh, Thomas Gaillard, Julien Schmitt, Corine Gerardin, Gaulthier Rydzek, Tangi Aubert

Hybrid silica cage-type nanostructures made from triply hydrophilic block copolymers single micelles

Anu Vashishtha[1], Anthony Phimphachanh[1], Thomas Gaillard[1], Julien Schmitt[1,2], Corine Gerardin[1], Gaulthier Rydzek[1,*], Tangi Aubert[1,*]

[1] ICGM, Univ Montpellier, CNRS, ENSCM, 34000 Montpellier, France.
[2] LSFC, CNRS, Saint-Gobain Research Provence, 84300 Cavaillon, France.

* E-mails : gaulthier.rydzek@umontpellier.fr, tangi.aubert@umontpellier.fr

Abstract
Controlling the structure and functionality of porous silica nanoparticles has been a continuous source of innovation with important potential for advanced biomedical applications. Their synthesis, however, usually involves passive surfactants or amphiphilic copolymers that do not add value to the material after synthesis. In contrast, polyion complex (PIC) micelles based on hydrophilic block copolymers allow for the direct synthesis of intrinsically functional hybrid materials. While most previous studies have focused on bulk materials made from double-hydrophilic block copolymers (DHBC), in this work we have synthesized a triple-hydrophilic block copolymer (THBC) and demonstrated both its PIC micellization and its potential for hybrid mesoporous silica nanomaterials. Introducing this THBC has allowed to direct the transition from bulk 3D materials to 0D nanomaterials with cage-type structures. The stabilization and isolation of these nanostructures formed around discrete individual micelles has been made possible by the careful design of the three different blocks that each play a key role. These nanostructures could also be synthesized from hybrid PIC micelles based on THBC-multivalent metal ions complexes, offering a direct route to metal/silica composite nanoparticles. This class of THBC polymers therefore creates significant opportunities for the synthesis of nanostructures with complex and functional architectures.

Keywords: mesoporous materials, colloids, polyion complex micelles, nanocages, SAXS

Porous silica nanoparticles have become highly relevant materials in the fields of nanomedicine for their potential in targeted drug delivery strategies and other theranostics applications.[1–5] The development of materials for such advanced applications demands a high degree of control over particle size, structure and functionalities in order to address important requirements such as large effective pore volumes, stability in biological media, or the ability to cross natural barriers.[6–8] To this end, the synthesis of porous silica nanoparticles through micelle soft-templating is a method of choice for the deliberate tailoring of particle size, shape and pore texture. Recent progress in this field has led to the formation of low-dimensional structures from single micelle systems.[9–11] Ultrasmall silica cages, in particular, were synthesized from individual hexadecyltrimethylammonium bromide (CTAB) micelles, and their structure was resolved by single particle reconstruction from electron microscopy images, revealing well-defined dodecahedral cage structures.[12] The formation of these calibrated nanostructures relies on a precise control of the interactions between the silica species and the micelles, and of their concerted co-assembly mechanism that leads to mesostructured materials.

Among the variety of structuring agents, amphiphilic block copolymers have shown great value to control the growth and structure of inorganic materials.[13] Their synthesis by design enables a virtually limitless combination of blocks with different characteristics and properties. The controlled self-assembly of these block copolymers has hence resulted in a diversity of mesostructured materials with

tailored properties, from energy storage to emerging quantum materials.[14,15] In this context, polyion complex (PIC) micelles are emerging as alternative structure directing and functionalizing agents to traditional surfactant or polymer micelles, which benefit from even more versatility of composition than amphiphilic block copolymers. PIC micelles are formed by the complexation of a multi-hydrophilic block copolymer containing at least a neutral block and an ionizable block, typically a polyacid, with a micellization partner of opposite charge, typically a polybase such as oligochitosan.[16] The formation and dissociation of such micelles can be controlled by pH (in the case of weak polyelectrolytes), temperature[17] or ionic strength.[18] Making use of these features, PIC micelles based on double hydrophilic block copolymers (DHBCs) in particular have been investigated as nanocarriers for biomedical applications.[19] Although the DHBCs are fully hydrophilic macromolecules by design, the complexation of their polyelectrolyte block drives the self-assembly of core-corona micelles. Their core is composed of a water-rich complex coacervate,[20] and their corona comprises the neutral block of the DHBC, which is hydrophilic and immiscible with the polyelectrolyte complex, and ensures the micelles solubility and stability in aqueous environments. PIC micelles based on DHBCs featuring ethylene oxide (EO) units on the neutral block have also been extensively used for the synthesis of mesoporous silica materials by co-precipitation methods.[21] These PIC micelles offer a versatile platform to modulate the structure and functionality of mesoporous silica materials by adjusting the nature, molecular weight, and volume fraction of each block. This freedom in the design of the block copolymer composition has enabled the synthesis of mesoporous silica materials with large pores[22] and varying pore structures, including 2D hexagonal, lamellar, wormlike or cage-type mesoporous silica.[23–25] This approach, however, has so far been limited to the production of bulky materials in the form of powders, with limited control on the particle size and shape. Recent work by Richard *et al.* showed that mixing two different DHBCs could lead to the formation of mixed PIC micelles, which resulted in a substantial reduction of the overall material size, down to a few hundreds of nanometers.[25] Such particle sizes are, however, still too large for many potential applications, for instance in drug delivery approaches.

Inspired by this work, we introduce herein a triple-hydrophilic block copolymer (THBC), namely poly(acrylamide)-*b*-poly(acrylic acid)-*b*-poly(oligo(ethylene glycol)-methyl ether acrylate), noted PAm-*b*-PAA-*b*-POEGMEA, for the formation of PIC micelles as the structure directing agent of mesoporous silica materials. The use of this triblock copolymer led to the formation of 0D mesoporous silica nanoparticles formed around individual micelles and without 3D periodicity of the porosity. We show, through a combination of transmission electron microscopy (TEM) and small angle X-ray scattering (SAXS) analyses, how the rational design of the polymer architecture played a key role in the formation of these 0D nanostructures. This terpolymer structure allows to deliberately mediate the interplay between silica growth and micelle interactions, and to control the ensuing self-assembly process that leads to nanoparticle formation. With this approach, we obtained sub-50 nm nanoparticles with cage-type structures and large pore sizes. In addition, thanks to the freedom in copolymer composition, the size of these cage-type nanostructure could be varied by changing the molecular weight ratio of the different blocks, which is a considerable advantage of block copolymers over classic surfactants.

Next to size control, our work also showcases the potential of these mesoporous nanostructures to serve as nanocarriers by loading them with actives species. Indeed, another asset of PIC micelles is that the neutral block remains anchored in the pore walls, resulting in mesoporous silica intrinsically grafted with a block copolymer, hence providing a direct route to functional materials. The nature of the blocks and of the micellization auxiliary can then be adapted to specific functional applications. For instance, DHBC micelles using a Pt^{II} compound[26] as the micellization agent, or tripartite micelles with additional siRNA,[27] have already been reported for biomedical applications. This strategy can also readily be applied to PIC-derived porous silica materials, which can then take advantage of pH controlled micelle dissociation for release mechanisms.[28] Here, the versatile loading of the THBC-based porous silica nanoparticles is demonstrated by replacing the common polybase micellization agent with multivalent metal ions, either before or after the synthesis of the silica nanostructures.

RESULTS AND DISCUSSION

THBC polymer synthesis. The reversible addition-fragmentation chain-transfer (RAFT) polymerization method is a powerful tool for the synthesis of specifically designed block copolymers with controlled molecular weights and low polydispersity indexes. This method has been extensively used for the synthesis of a variety of DHBC copolymers.[29] In this work, we designed and synthesized a PAm-*b*-PAA-*b*-POEGMEA triblock copolymer by aqueous RAFT polymerization (Scheme 1). This THBC was synthesized using 2-(butylthiocarbonothioylthio)-2-methylpropanoic acid (BDMAT) as the chain transfer agent and 4,4'-azobis(4-cyanopentanoic acid) (ACPA) as the radical initiator. First, acrylamide monomers were polymerized into a PAm block that was then used as a macro-chain transfer agent for the subsequent PAA and POEGMEA blocks. The reaction products were analyzed by ^{1}H NMR after each polymerization step (Figure S1), confirming a nearly total (*ca.* 98%) conversion of monomers into polymers. The number average molecular weight (M_n) and degree of polymerization of each block were estimated from the ^{1}H NMR data based on the corresponding peak areas for each block. These results confirmed the successful sequential polymerization of the three blocks (Figure S1) and were corroborated by the mass ratios of the C and N elements calculated from elemental analyses (Table S2). The synthesis described in the experimental section resulted in a THBC composition of PAm_{144}-*b*-PAA_{52}-*b*-$POEGMEA_{29}$, which corresponds to molecular weights of 10.2 kg/mol, 3.7 kg/mol and 13.9 kg/mol for the PAm, PAA and POEGMEA blocks, respectively. The polydispersity index (M_w/M_n) of this THBC was estimated to 1.14 by aqueous size exclusion chromatography with a multi angle laser light scattering detector (SEC-MALS), considering a monomodal distribution of the polymer chains (Figure S2). For comparison purpose, a DHBC polymer with comparable blocks, namely PAA_{45}-*b*-$POEGMEA_{24}$, was also synthesized based on an existing procedure.[30] The chemical structures of these DHBC and THBC polymers are illustrated in Figure 1a. Other THBC polymers with varying compositions were also synthesized in this work to investigate the role of each block. The details of all the polymers are provided in the Supporting Information, Table S1.

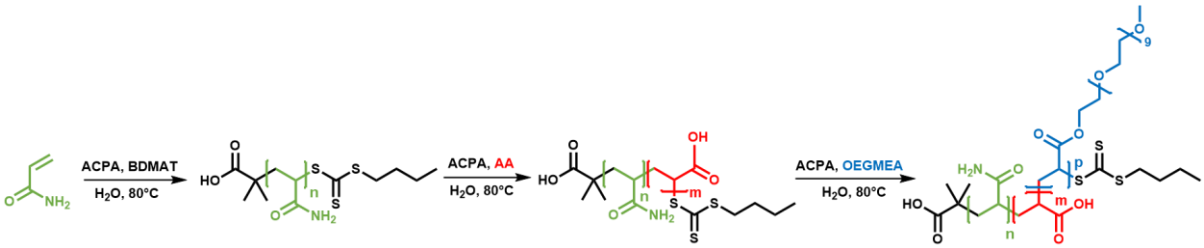

Scheme 1. Synthesis by RAFT polymerization of PAm_n-*b*-PAA_m-*b*-$POEGMEA_p$ THBC.

Formation of PIC micelles based on THBC copolymer. Next to the successful synthesis of the THBC polymer, its ability to form PIC micelles had to be confirmed. This process, which is well documented for DHBC polymers,[29] is illustrated in Figure 1b in the case of oligochitosan as the complexation partner. At slightly acidic pH, protonated ammonium groups of oligochitosan interact electrostatically with acrylate groups of the PAA block, forming a coacervate phase that defines the PIC micelle core, surrounded by a POEGMEA corona. Since both PAA and oligochitosan are weak polyelectrolytes, the subsequent dissociation of the PIC micelles under pH conditions where the charge of one of the partners is neutralized has also been demonstrated, hence making it a reversible process.[16] The formation of such PIC micelles using a fully hydrophilic triblock copolymer, however, had so far not been reported. To investigate the micellization ability of THBC, PAm_{144}-*b*-PAA_{52}-*b*-$POEGMEA_{29}$ was solubilized with oligochitosan in water. For consistency, in this work the molar concentration of ethylene oxide (EO) groups from POEGMEA was systematically set to 0.1 M, which corresponds to a weight fraction of *ca.* 1 wt% of copolymer in the case of THBC. In addition, the concentration of oligochitosan was set to have an equimolar ratio between the amine and acrylic acid groups (N:AA = 1) from the oligochitosan and the copolymer, respectively. The pH of the resulting mixture was then

adjusted in the range 2 to 8 to cover conditions where either both or only one of the polyelectrolytes are ionized, and the suspensions were analyzed by SAXS (Figure 1d). An emerging signal is observed when changing the pH from 2 (where the PAA block is uncharged) to 4.5 (where both PAA and oligochitosan are charged) before decreasing again up to pH 8 (where oligochitosan is uncharged). This variation in the scattering pattern is associated to the formation of the micelles by electrostatic complexation between the THBC and oligochitosan, with an optimum at pH 4.5. This is further demonstrated by comparing the signals from THBC polymer alone in aqueous solution and the THBC/oligochitosan mixture at pH 4.5 (Figure 1e). In the absence of oligochitosan, a THBC polymer aqueous solution at the same concentration typically shows a low scattering pattern, with an intensity at zero scattering angle (I_0) of *ca.* 0.1 cm^{-1}. In contrast, the SAXS pattern of the THBC/oligochitosan mixture at pH 4.5, under conditions where both polyelectrolytes are ionized, is characterized by a much stronger signal, with a plateau at low q values associated to an I_0 of *ca.* 3 cm^{-1}. This plateau is followed by a drop in intensity at *ca.* q = 0.2 nm^{-1}, and at even higher q values, by a well-defined slope corresponding to a power law of $I \propto q^{-2}$. These characteristic features are a clear signature of the formation of micelles with a well-defined core whose interface with the diffuse corona is clearly marked. In addition, the SAXS pattern at pH 4.5 does not exhibit any structure factor that would have suggested inter-micelle interactions, which confirms that the solution consists of discrete and colloidally stable PIC micelles. The SAXS patterns at different pH values were further analyzed based on the Guinier approximation using BioXTAS RAW program in order to estimate more accurately their I_0.[31] At constant polymer concentration, and in the absence of any structure factor, I_0 scales with the molecular weight of the scattering species, thus, higher I_0 values typically reflect higher aggregation numbers or higher proportions of micellized polymer chains (*i.e.*, less free polymer chains). The evolution of I_0 as a function of pH (Figure 1f) hence confirms the existence of an optimal micellization window in the pH range 4 to 6.5 for the THBC/oligochitosan system. This pH range corresponds to conditions where both oligochitosan and PAA are ionized, which is consistent with the reversible micellization behavior previously reported for conventional DHBC/oligochitosan systems.[29] We can therefore reasonably expect that THBC-based PIC micelles are following a similar self-assembly mechanism, illustrated in Figure 1c, with the PIC micelle core consisting of a PAA/oligochitosan coacervate stabilized by a neutral hydrophilic corona comprising the PAm and POEGMEA blocks. The radius of gyration (R_g) of the THBC-based PIC micelles resulting from the Guinier analysis of their SAXS pattern was estimated to 6.4 nm at pH 4.5, as compared to 3.7 nm for the free THBC. In addition, the SAXS pattern of the THBC/oligochitosan mixture at pH 2 (Figure 1d) shows a pattern highly similar to the one of THBC alone, confirming that no micelles are formed when the THBC is uncharged. The ratio of I_0 at pH 4.5 and 2 can therefore be used to determine the aggregation number, which is estimated to 20 for this THBC/oligochitosan duo.

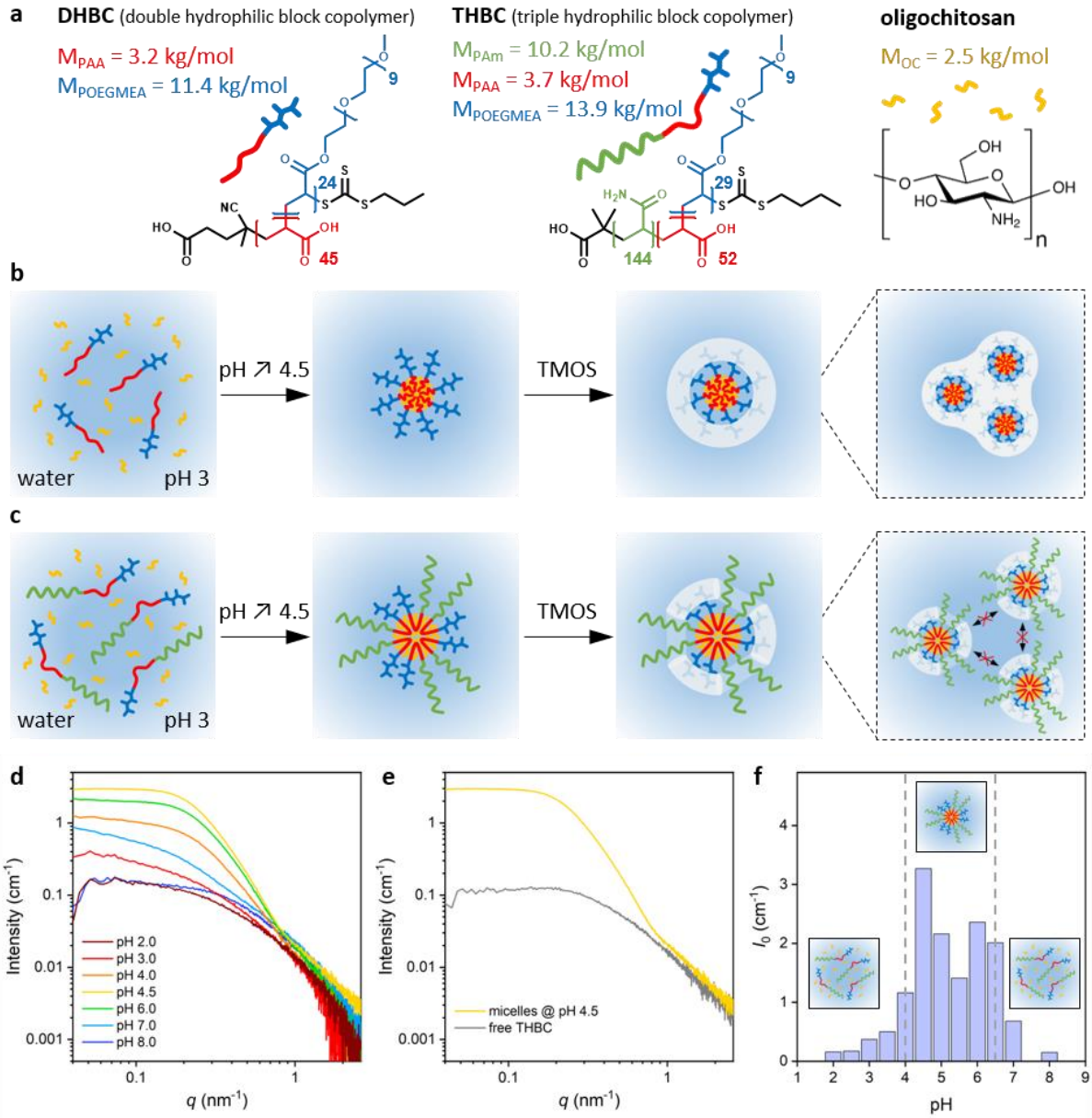

Figure 1. (a) Topological chemical structures of DHBC, THBC, and oligochitosan under their non-ionized forms. Illustration of (b) DHBC-based, and (c) THBC-based PIC micelles self-assembly, and their interaction with condensing silicic species (white domains) during the sol-gel process, yielding either 3D or 0D (nano)structured silica. (d) SAXS patterns of the THBC/oligochitosan mixture ([EO] = 0.1 M, N:AA = 1) as a function of pH. (e) SAXS patterns of the THBC polymer alone and micelles formed at pH 4.5 ([EO] = 0.1 M in both cases). (f) Intensity at zero scattering angle (I_0) as a function of pH (dashed lines indicate the pH window in between the pKa values of PAA and oligochitosan where electrostatic interactions are favored). The SAXS data are displayed in absolute scale.

From bulk 3D mesoporous silica to 0D cage-type nanostructures. Hybrid mesoporous silica materials were thereafter synthesized through a sol-gel process in the presence of THBC and/or DHBC-based PIC micelles, with oligochitosan as the complexation partner for micellization. This sol-gel synthesis relies on the hydrolysis of an alkoxysilane precursor, followed by the condensation of silicic species. Tetraethyl orthosilicate (TEOS) is probably the most common alkoxysilane used for this purpose, but is not readily miscible with water. Thus, common approaches for the synthesis of mesoporous silica from DHBC-based PIC micelles and TEOS usually make use of a two-step procedure involving first the hydrolysis of TEOS at pH < 3, followed by the micellization and condensation reaction

at pH 4-6.[29] In this work, the synthesis of PIC-based mesoporous silica was adapted to provide a simpler one-step procedure, illustrated in Figure 1c. To this end, TMOS was used as the silica precursor for its higher water miscibility and faster hydrolysis rate as compared to TEOS. The addition of TMOS to PIC suspensions resulted in almost immediate homogenous mixing with water at pH 4.5, hence considerably facilitating the synthesis and improving reproducibility. In the presence of PIC micelles, the hydrolyzed silicic species then interact with the ethylene oxide units of the POEGMEA block, leading to a co-assembly of the micelles with silica. Thus, in addition to maintaining [EO] = 0.1 M and N:AA = 1, the synthesis conditions of mesoporous silica were also systematically set to an equimolar ratio between the silicic and ethylene oxide groups (Si:EO = 1, see experimental section for full synthesis details). Performing this synthesis with a conventional DHBC, namely PAA_{45}-*b*-$POEGMEA_{24}$, resulted in the macroscopic precipitation of a bulky material, which, upon TEM analysis (Figure 2a), shows ordered mesoporosity with a 2D hexagonal structure (*p6mm* symmetry) made of cylindrical pores. This observation is consistent with previous works on bulk mesoporous silica made from DHBC-based PIC micelles, and is explained by the interaction of EO units with silanol groups of silicic species, resulting in a cooperative self-assembly of PIC micelles with silica.[16,32] From this point, a fraction of DHBC was gradually substituted with THBC in the synthesis, while maintaining constant the overall molar amount of EO groups (n_{EO}) coming from the POEGMEA block. The THBC fraction is then defined as $\%THBC = n_{EO,THBC}/(n_{EO,THBC} + n_{EO,DHBC})$. The Si:EO ratio was kept to 1, ensuring a constant concentration of silica throughout the experiments. As evidenced in Figure 2, the introduction of THBC in the PIC micelles resulted in a radical decrease of the particle size, from bulky particles at 0% THBC to well-defined nanoparticles of about 40 nm at 100% THBC. Along with the particle size, the number of pores per particle also decreases, evolving from particles with multiple pores and some degree of ordering (30% THBC, Figure 2d), to single pore nanoparticles with no periodicity (100% THBC, Figure 2f). The nanoparticles obtained from 100% THBC are also characterized by a hydrodynamic diameter of about 60 nm, which is significantly larger than their 40 nm physical diameter. The TEM observation of isolated nanoparticles revealed the presence of an organic corona around the silica nanoparticles (Figure S3). This corona, which explains the larger hydrodynamic diameter, most likely consists of the PAm blocks that stretch out from the nanoparticles, hence providing colloidal stability as discussed later in the article. This finding is in line with the recent work of Richard *et al.* who demonstrated the preferential localization of PAm blocks on the outer surface of silica particles.[25] The nanoparticles obtained from 100% THBC were further investigated by TEM to resolve the structure of their inorganic component.

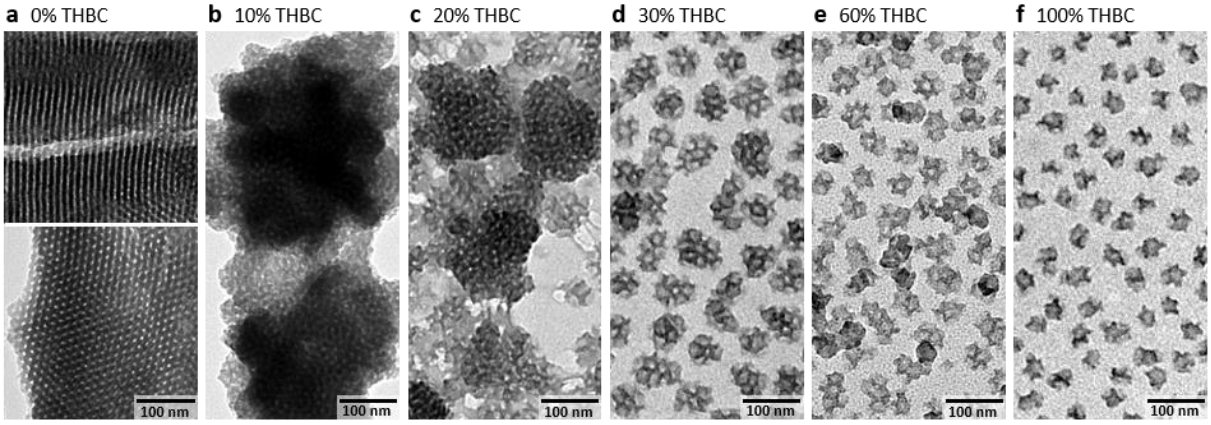

Figure 2. TEM images of mesoporous silica obtained using DHBC/THBC/oligochitosan PIC micelles with a copolymer composition of (a) 0% THBC (*i.e.* 100% DHBC, images from two different areas of microtome sections), (b) 10% THBC, (c) 20% THBC, (d) 30% THBC, (e) 60% THBC, and (f) 100% THBC (images acquired at 100 kV, *ca.* 0.4 nm/pix).

Structural resolution of 0D cage-type nanostructures. Figure 3a shows a TEM image of nanoparticles obtained from 100% THBC with composition PAm_{124}-*b*-PAA_{50}-*b*-$POEGMEA_{22}$, and acquired with a higher resolution camera (0.2 nm/pix). These nanoparticles have an average diameter of about 40 nm and appear to be made of struts, with some showing repeating patterns from particle to particle, suggesting an underlying symmetry. We therefore attempted to resolve the structure of these nanoparticles through single particle 3D reconstruction using EMAN2.9 software.[33] For this reconstruction process, about 11k single particle images were isolated by a neural network particle picker (Figure 3b,c).[34] These single particle images were then aligned and averaged in 64 classes based on their similarities (Figure 3d). A volumetric model was thereafter generated by single particle refinement[35] (Figure 3e). For this refinement, an icosahedral symmetry was assumed, which could be reasonably expected based on previous work.[12] The resulting 3D model suggests that some of the particles have a structure consistent with a dodecahedral cage, although other structures are most likely present as well in the sample. The material hence consists of cage-type nanoparticles that are formed from single or limited number of micelles. These cages are the same ones that take part in the structuration of some 3D bulk mesoporous silica materials,[36] with the dodecahedral cage probably being the most common one. In line with the absence or pore periodicity observed by TEM, these nanoparticles obtained from 100% THBC can be seen as the 0D version of cage-type mesoporous silica materials.

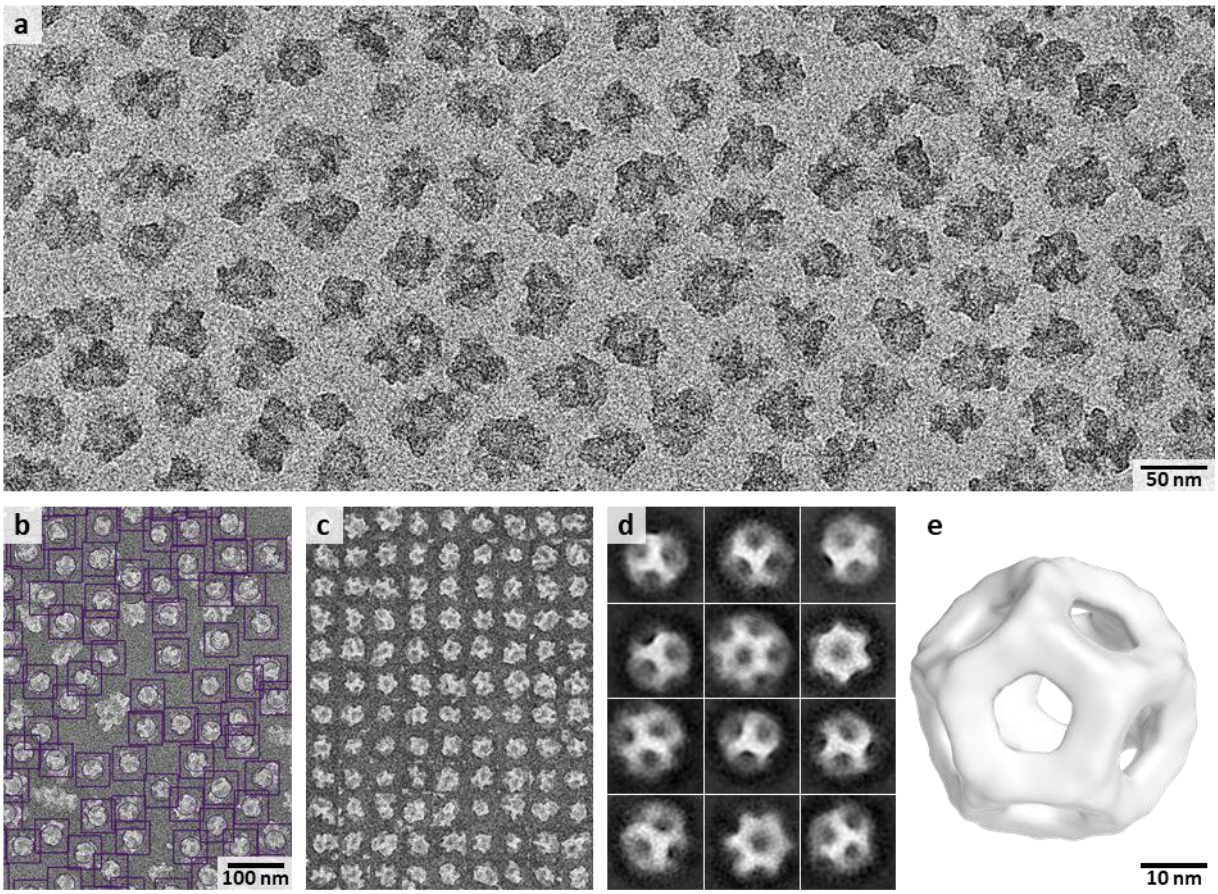

Figure 3. (a) TEM image of 0D mesoporous silica nanoparticles obtained from THBC/oligochitosan PIC micelles (acquired at 120 kV, *ca.* 0.2 nm/pix). Illustration of the single particle 3D reconstruction process, involving (b) automated particle picking to generate (c) a large set of single particle images (contrast is inverted, not all particles are shown), which are then averaged into (d) 64 classes (12 of them are shown), that serve as the basis for (e) the refined 3D model of the cage-type structure (visualized by UCSF Chimera[37]).

SAXS monitoring of the structural evolution from 3D mesoporous silica to 0D cage-type nanostructures. The progressive transition from 3D to 0D mesoporous materials by replacing DHBC with THBC was further monitored through SAXS (Figure 4). First, suspensions of PIC micelles with different fractions of PAm_{144}-*b*-PAA_{52}-*b*-$POEGMEA_{29}$ THBC were studied (Figure 4a). Similarly to the THBC micelles presented in Figure 1, micelles based on DHBC only (0% THBC) are also characterized by an oscillation at *ca.* q = 0.2 nm^{-1}. The SAXS pattern of these DHBC micelles, however, exhibits an increase in intensity at the smallest angles, which could be signature for long-range attractive interactions between micelles. On increasing THBC fractions, the characteristic onset of the Guinier plateau of the micelle form factor shifts towards lower *q* values, indicating an increase in the radius of gyration, from R_g = 5.5 nm with 100% DHBC to 6.4 nm with 100% THBC. For comparison, these micelles were also observed by TEM via negative staining of the samples (Figure S4), showing spherical micelles with average diameters of 16 nm and 22 nm for the DHBC and THBC micelles, respectively. Thus, while suggesting slightly larger sizes these TEM observations also confirm the increase in micelle size from DHBC to THBC observed by SAXS. In addition, the attractive interaction feature in the SAXS pattern at low *q* is decreasing with increasing THBC fractions, ultimately becoming a plateau for micelles with 100% THBC, evidencing the absence of interactions in this case. We note that the micelle sample with 30% THBC shows inconsistent behavior at low *q* (Figure 4a), which could be due to some inhomogeneity generated during sample preparation. Next, SAXS measurements of the as-prepared hybrid mesoporous silica materials synthesized from different fractions of PAm_{144}-*b*-PAA_{52}-*b*-$POEGMEA_{29}$ THBC were carried out (Figure 4b,c). In line with the TEM observations, the SAXS pattern of the silica material obtained from PIC micelles based on DHBC (0% THBC) exhibit a clear structure factor, with the emergence of Bragg peaks from the material organization (Figure 4b). The corresponding Iq^4 vs. *q* plot (Figure 4c) highlights the main scattering peaks at 0.40, 0.70, and 0.80 nm^{-1}, which can be assigned to the (10), (11), and (20) peaks, respectively, of the *p6mm* symmetry. A second *p6mm* structure at slightly higher *q* values can also be noted, which could be due to some polydispersity of the DHBC. As the fraction of THBC gradually increases, a decrease in the peak intensities is observed, associated with a broadening of the peak shape, which is in line with a decrease of the ordered domains extension and hence the reduction of the material size seen in TEM. Concurrently, the (10) peak shifts from 0.40 nm^{-1} at 0% THBC to 0.33 nm^{-1} at 80% THBC, which corresponds to an increase of the lattice parameter from 16 nm to 19 nm. This increase in lattice parameter also suggests a concomitant increase of the pore size when replacing the DHBC with THBC. In the low *q* domain, below 0.2 nm^{-1}, the SAXS pattern of the 3D structure (0% THBC) shows a power law with an exponent of -4, indicating a sharp external surface of the bulky mesoporous material. Increasing the THBC fraction induces a progressive decrease of this slope, with the apparition of a Guinier plateau at 100% THBC. In this case, the SAXS pattern is free of any structure factor. The (10) peak has completely disappeared, highlighting the absence of long-range order, and the form factor could be fitted, for *q* values up to 0.5 nm^{-1}, with a simple sphere model with no interaction contribution (Figure S5), in line with the high colloidal stability of the suspensions. The fit resulted in a diameter of 48 nm for the sphere model, which matches well the average size of 50 nm estimated by TEM for nanoparticles obtained with that PAm_{144}-*b*-PAA_{52}-*b*-$POEGMEA_{29}$ THBC.

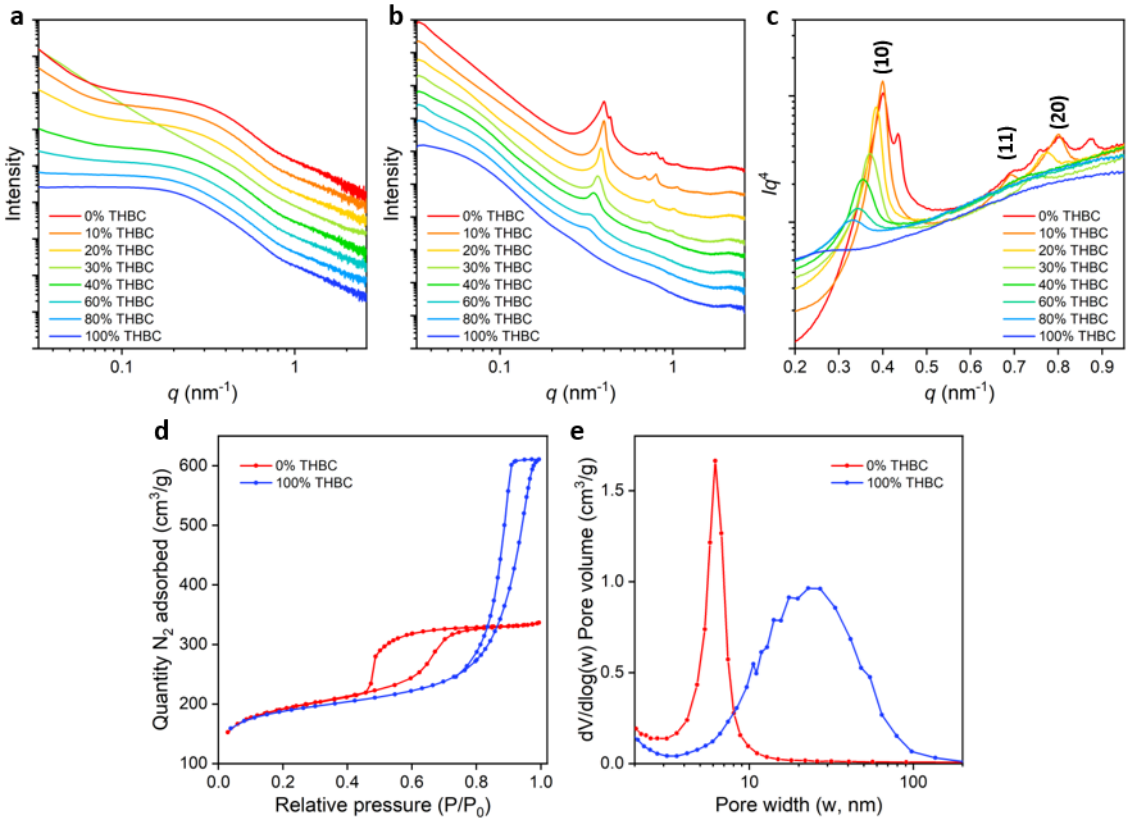

Figure 4. SAXS patterns of (a) PIC micelles, and (b) PIC-based mesoporous silica suspensions for different fractions of THBC (pH 4.5, [EO] = 0.1 M, data are offset for clarity). (c) Evolution of Iq^4 as a function of q for the SAXS pattern of mesoporous silica suspensions. (d) Nitrogen sorption isotherms of calcined 0D mesoporous silica nanoparticles obtained from 100% THBC/oligochitosan PIC micelles and 3D mesoporous silica obtained from DHBC/oligochitosan PIC micelles. (e) Corresponding pore size distributions as determined by the BJH method.

The structural evolution from 3D to 0D mesoporous silica was also investigated in terms of specific surface area and pore size distributions using nitrogen sorption analyses (Figure 4d). Prior to measurements, the porosity of the mesoporous silica materials was released by calcination at 550 °C in air for 6 hours. Both 3D and 0D materials show type IV isotherms, which is a classic signature for mesoporous materials, and have very similar specific surface areas, specifically 645 and 625 m^2/g for the 3D and 0D mesoporous silica, respectively. The position of the hysteresis, on the other hand, shifts to higher relative pressures from 3D and 0D materials. In the case of 3D mesoporous silica, the corresponding average pore size was estimated to 6 nm with a narrow distribution as determined by the Barrett-Joyner-Halenda (BJH) method on the adsorption branch (Figure 4e). In the case of 0D mesoporous silica, an estimate from BJH method gave an average pore size of 20 nm with a broad distribution that most likely covers both the nanoparticle inner porosity as well as the porosity formed by inter-particulate voids. In addition, the BJH method implies some assumptions on the pore geometry that may not describe our nanomaterial very well. Nevertheless, this result still reflects the significant difference in pore size between the two systems.

A tentative model for the formation of 0D nanostructures: role of the different blocks. Both the SAXS and TEM analyses highlight the emergence of stable colloids composed of hybrid mesoporous silica nanoparticles when the proportion of THBC used in PIC micelles is increased, ultimately yielding 0D mesoporous nanoparticles. It is therefore clear that the chemical structure of the THBC plays a crucial role in the formation, size control and colloidal stabilization of the 0D nanostructures. In the case of PAA-*b*-POEGMEA DHBC-based PIC micelles, the formation of 3D mesoporous silica is well

explained by the interaction of silicic species with the EO groups of the POEGMEA block through hydrogen bonds,[25] resulting in a concerted co-assembly of multiple micelles with silicic species and a subsequent unrestricted growth of the resulting hybrid material (Figure 1b). In contrast, it was recently proposed that the growth of mesostructured PIC-based silica materials could be limited when using PAA-*b*-PAm DHBC polymers as capping agents, in combination with the usual PAA-*b*-POEGMEA, to form mixed PIC micelles.[25] The rationale behind this strategy is that the inability of PAm to interact with silicic species, combined with its lack of interaction with PAA in the pH range 4-6, would allow DHBC containing highly water-soluble PAm to preferentially locate at the surface of multi-micelle mesostructured silica particles and act as a stabilizing neutral corona in water. However, this approach failed to produce mesoporous particles with a diameter smaller than a few hundred nanometers.

In this work, the THBC was designed to comprise both the silica-interacting (*i.e.*, POEGMEA) and the capping blocks (i.e., PAm), covalently linked to the central complexing block (*i.e.*, PAA). This constrained geometry implies that each THBC-based PIC micelle is capable of both promoting and confining silica growth, unlike mixed PIC micelles made of two DHBCs, which can be more or less rich in PAm. Therefore, in THBC-based micelles, the PAm block induces steric hindrance within the system, hampering the assembly of multiple micelles (Figure 1c). Thus, using PAm-*b*-PAA-*b*-POEGMEA THBC copolymer enables confining the material growth to the single micelle level while simultaneously templating the silica porous structure. After sol-gel condensation, the PAm block further confers high colloidal stability to the resulting nanoparticles in aqueous solution, as testified by the absence of interaction between colloids evidenced by SAXS analyses (Figure 4b). It should be noted that the order of the blocks in the copolymer is also crucial for the formation of structured materials. In particular, the PAA block should be in the middle of the copolymer chain. Attempts at synthesizing silica materials from a PAm-*b*-POEGMEA-*b*-PAA THBC (*i.e.*, inverting the position of the POEGMEA and PAA blocks, all other synthetic parameters remaining the same) resulted in the macroscopic precipitation of ill-defined materials without any apparent structuring (Figure S6).

To verify this tentative model of the role of the PAm block, a series of THBCs with varying block M_n were synthesized and the resulting copolymers were tested for the sol-gel synthesis of mesoporous silica nanoparticles. The structural properties of the obtained materials were examined in the light of two parameters: (i) the M_n of the PAm block, and (ii) the PAm/POEGMEA mass ratio. The mass of the ionizable block (PAA) was kept constant at around 3 kg/mol. In line with the above proposed model, Figure 5 confirms that a minimal PAm molecular weight is required to prevent the formation of large multi-micelles structures. For instance, a 5.3 kg/mol PAm block gave a bulky material with poor structuration (Figure 5a). Slightly longer PAm blocks (5.6-6.5 kg/mol) started to produce nanoparticles, but with elongated shapes and unclear pore structures (Figure 5b,c). It is only for a PAm block of 8.8 kg/mol and above that 0D cage-type nanostructures were obtained (Figure 5d-f). Conversely, varying the molecular weight of the POEGMEA block resulted in the opposite effect (Figure S7). Using a lower molecular weight POEGMEA block (7.2 kg/mol) resulted in homogeneous 0D nanostructures, but with thin silica walls due to a low amount of EO (and thus Si) per micelle. Increasing the molecular weight of the POEGMEA block, however, progressively increased the material dimensions, yielding multi-pore nanoparticles at 20.2 kg/mol, and particles exceeding 100 nm with poor structuration at 31.2 kg/mol. Next to the absolute M_n of each block, the corresponding mass ratios between PAm and POEGMEA blocks should also be considered. For instance, in Figure 5d the particles are larger than in Figure 5e in spite of the larger PAm block, as this specific polymer also has a larger POEGMEA block. A PAm block above 8 kg/mol is also not a sufficient condition alone and non-0D materials may be obtained if the POEGMEA block is very large (Figure S7d). From all the tested THBC compositions, it appears that a PAm/POEGMEA molecular weight ratio above *ca.* 0.7 seems to be required for the formation of 0D cage-type nanostructures. Given the linear versus brush structure of the PAm and POEGMEA blocks, respectively, this ratio in terms of degree of polymerization is close to 5, which highlights the importance of having a significantly longer PAm block for an efficient capping effect. This ratio was also found to have a direct incidence on the size of the nanostructures, with average diameters of *ca.* 50 nm, 40 nm and 35 nm for nanomaterials synthesized from THBCs having PAm/POEGMEA ratios of

0.73, 0.83 and 1.38, respectively (Figure 5d-f). The average sizes and hydrodynamic diameters of 0D nanoparticles obtained from different polymers are summarized in Table S3. The ability to control the size of the nanoparticles is a considerable advantage of block copolymers, which offer much more freedom to modulate the material properties, compared to conventional surfactants.

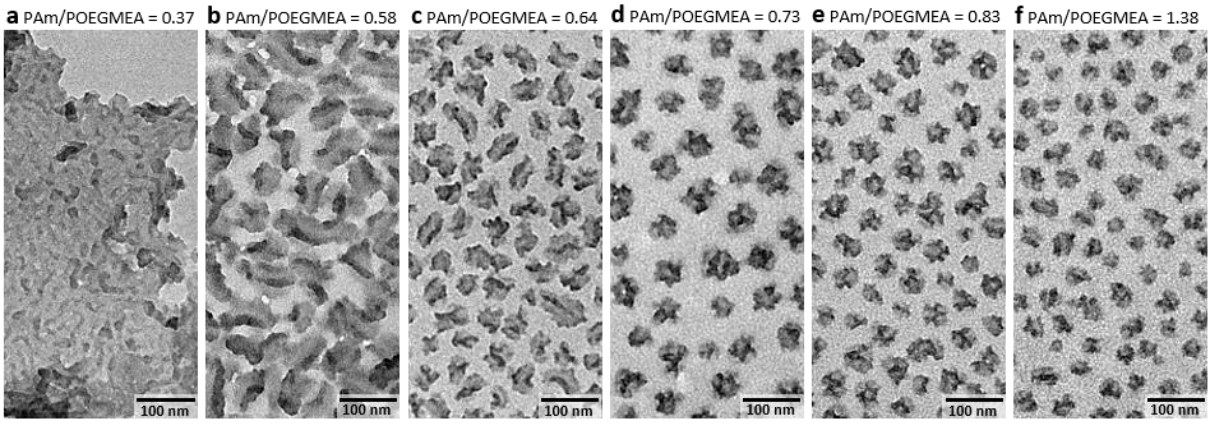

Figure 5. TEM images of silica materials obtained from PIC micelles based on (a) PAm(5.3k)-*b*-PAA(3.3k)-*b*-POEGMEA(14.4k), (b) PAm(5.6k)-*b*-PAA(3.2k)-*b*-POEGMEA(9.6k), (c) PAm(6.5k)-*b*-PAA(3.6k)-*b*-POEGMEA(10.1k), (d) PAm(10.2k)-*b*-PAA(3.7k)-*b*-POEGMEA(13.9k), (e) PAm(8.8k)-*b*-PAA(3.6k)-*b*-POEGMEA(10.6k), and (f) PAm(15.2k)-*b*-PAA(3.0k)-*b*-POEGMEA(11.0k). The corresponding PAm/POEGMEA molecular weight ratios are indicated above each image.

Intrinsically functional hybrid mesoporous silica nanomaterials. One of the great assets of PIC-derived mesoporous silica is that the POEGMEA blocks remains anchored to the silica walls after synthesis, yielding hybrid THBC-functionalized materials. The silica nanostructures reported here hence bear carboxylate groups from the PAA block that can readily be used to load the nanoparticles with active species in view of functional applications. To demonstrate this potential, we used these carboxylate groups to load Cu^{2+} ions in the nanoparticles (Figure 6a). To this end, we dissolved $CuCl_2$ in a solution of silica nanoparticles synthesized with 100% of PAm_{124}-*b*-PAA_{50}-*b*-$POEGMEA_{22}$ THBC. The amount of $CuCl_2$ was calculated to have an equimolar ratio of copper to acrylate groups (Cu:AA = 1), and by considering that no THBC was lost during the synthesis. The solution was left to stir for 4 hours and the nanoparticles were then precipitated with ethanol and centrifuged (3600 g, 10 min), resulting in mostly colorless supernatant. Redispersing the obtained solid in the same volume of water yielded a very bright blue solution, characteristic of Cu ion species (Figure 6a). This process was monitored by UV absorption spectroscopy (Figure 6b), revealing the apparition of a distinct absorption feature at 260 nm upon adsorption of Cu^{2+} by the nanoparticles, which is initially not present in either the THBC/SiO_2 nanoparticles or $CuCl_2$ solutions. Mixing $CuCl_2$ with a solution of THBC alone at same ratio (Cu:AA = 1) also produced the same absorption band at 260 nm (Figure S8). This feature is hence consistent with the formation of a Cu/PAA complex as previously reported,[38] and confirms that Cu ion species are effectively loaded by interaction with the copolymer. This property of the THBC-functionalized silica nanoparticles is further reversible. Decreasing the pH of the solution to 2 with HCl protonates the carboxylates from PAA, which releases the Cu^{2+} ions and results in a colorless suspension after centrifugation and redispersion of the nanoparticles in water (Figure 6a). The corresponding UV spectrum no longer comprises the Cu/PAA feature at 260 nm, but only an absorption feature at 310 nm that originates from BDMAT, the chain transfer agent of the THBC (Figure S8). The UV spectrum after Cu ions release also shows an overall decrease in the absorption and scattering contributions in the UV, which is consistent with the significant loss of the initial yellow coloration. While it could be partially due to some loss of material during the successive centrifugation steps, it mostly reflects the removal of oligochitosan, which has a broad absorbance in the UV-blue

range (Figure S8), and further highlights how Cu ions replace the initial micellization partner by complexing with the PAA blocks.

Thus, while the use of Cu ions is a convenient approach to visually evidence the loading and release process, this strategy could be applied to other water-soluble compounds capable of complexing with carboxylate groups, such as therapeutic compounds for biomedical applications for instance.[39] Nevertheless, the silica nanoparticles can also be loaded with metallic species or other active species directly during their synthesis. Indeed, next to the block copolymer, the nature of the micellization agent can also be modified to change the properties of the resulting materials or to add functionalities on their own. In this regard, the formation of hybrid PIC micelles, or HPIC, has already been reported through the complexation of DHBCs with multivalent metal salts[40–42] instead of organic polybases such as the oligochitosan used so far in this work. Here, silica nanostructures were synthesized from HPIC micelles by replacing the oligochitosan with different metal salts in our synthesis of 0D nanomaterials, including $ZnCl_2$, $CoCl_2$, $NiCl_2$ and $MnSO_4$ salts. For these syntheses, we kept the same conditions as those described in the experimental section, with [EO] = 0.1 M, and calculated the amount of metal salt to have M:AA = 0.5 (M = Zn^{2+}, Co^{2+}, Ni^{2+}, or Mn^{2+}). The volume of NH_4OH was also adjusted to keep the pH at 4.5 for all syntheses. Using $ZnCl_2$ as the complexation partner led to the formation of well-defined cage-type nanostructures (Figure 6c). These nanoparticles show good homogeneity with very similar morphologies as those obtained with oligochitosan, which clearly indicates the good propensity of divalent Zn ions to form HPIC micelles with THBC. Using $CoCl_2$, $NiCl_2$ or $MnSO_4$ salts also resulted in discrete and stable nanoparticles (Figure 6d-f), although their shape is less well defined and their porous nature is not evident based on the TEM images. In addition, the nanoparticles obtained from $MnSO_4$ also show smaller sizes, *ca.* 25 nm, as compared to Zn, Ni and Co-based nanoparticles, which are about 50 nm, 55 nm and 60 nm, respectively. The average sizes and hydrodynamic diameters of these nanoparticles obtained from different micellization agents are summarized in Table S3.

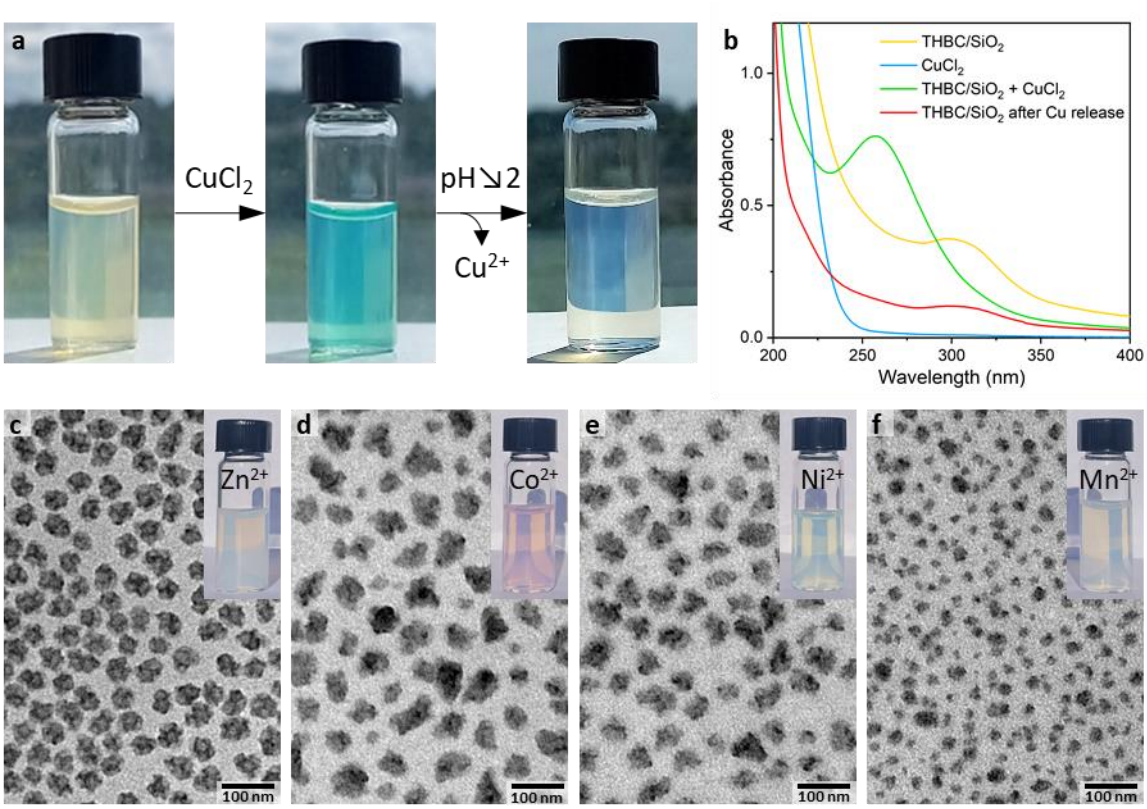

Figure 6. (a) Pictures of a THBC/SiO_2 nanoparticles solution as-synthesized (left), after the adsorption of Cu^{2+} (middle), and after the release of Cu^{2+} (right). (b) UV absorption spectra of the THBC/SiO_2 nanoparticles solution at the different steps of Cu^{2+} adsorption and release, and compared to the absorption spectra of aqueous solutions of $CuCl_2$ at comparable concentrations (the solutions were diluted 50 times in water). (c-f) TEM images of hybrid silica nanoparticles synthesized using (c) $ZnCl_2$, (d) $CoCl_2$, (e) $NiCl_2$, and (f) $MnSO_4$ as the micellization agent instead of oligochitosan (insets: pictures of the corresponding nanoparticle solutions). The nanoparticles in (c-f) were synthesized using PAm_{171}-*b*-PAA_{78}-*b*-$POEGMEA_{31}$ THBC.

CONCLUSIONS

In summary, we demonstrate here how triple-hydrophilic block copolymers provide a means of balancing the interactions between PIC micelles and silica species, which can be harnessed for the synthesis of precise porous silica nanomaterials. The PAm-*b*-PAA-*b*-POEGMEA THBC was specifically designed to combine three different blocks, each with its own critical role, including a block for PIC micelle core formation (PAA), a block for interaction with silica (POEGMEA) and a block for steric stabilization of nanostructures (PAm). In contrast to mixed DHBC systems, the use of a THBC having the highly hydrophilic PAm block on the same polymer chain as the silica-philic POEGMEA block has allowed for a maximal control of silica growth, which can then be confined around individual micelles. Based on our experiments, we can further provide guidelines for tailored polymer compositions. In our conditions, a PAm block above 8 kg/mol and a PAm/POEGMEA molecular weight ratio above 0.7 seem to be appropriate features for the synthesis of well-defined 0D cage-type nanostructures. Nevertheless, these guidelines may not be strict requirements and other conditions could potentially give rise to other valuable nanostructures. THBC-based PIC micelles also allow for larger pore sizes than cationic surfactants, such as CTAB, which typically result in sub-10 nm pore sizes. On the other hand, the synthesis of such 0D nanostructures from other common triblock non-ionic surfactants, such as pluronics, might prove impossible due to the symmetric structure of these amphiphilic block copolymers. Thus, single micelle systems with such large pore sizes are possibly only achievable with a terpolymer design such as the one reported here. These THBC-based PIC micelles therefore allow

for the engineering of complex nanoparticle architectures, taking advantage of the tunable composition of block copolymers. Combined with the versatile loading and release strategy enabled by their fully hydrophilic nature or their synthesis from HPIC micelles, these hybrid nanostructures constitute well-suited porous nanoplatforms for advanced functional applications in biotechnology and beyond.

EXPERIMENTAL SECTION

Materials. Oligochitosan with a molecular weight of 2500 g/mol and a deacetylation degree of 97% was purchased from Creative PEGWorks. Tetramethyl orthosilicate (TMOS, 99%), oligo(ethylene glycol)-methyl ether acrylate (OEGMEA, 99%, M_n = 480 g/mol, 9 EO units on average), 4,4'-azobis(4-cyano pentanoic acid) (ACPA, 98%), acrylamide (Am, 99%), acrylic acid (AA, 99%), D_2O, and anhydrous 1,4-dioxane (99.8%) were purchased from Sigma-Aldrich. Prior to their polymerization, any radical inhibitors were removed from monomers by sorption on alumina powder. Zinc chloride (98%), Nickel (II) chloride hexahydrate (97%), Manganese sulfate (97%), Cobalt (II) chloride hexahydrate (98%) and Copper (II) chloride dihydrate (99%) were purchased from Sigma-Aldrich. Ammonium hydroxide solution (28% in water) was purchased from VWR Chemicals. The polymerization chain transfer agents, namely 2-(butylthiocarbonothioylthio)-2-methylpropanoic acid (BDMAT) and 4-cyano-4-thiothiopropylsulfanyl pentanoic acid (CTPPA), were synthesized based on routine procedures published elsewhere.[43,44] All syntheses were carried out using Milli-Q water with a resistivity of 18.2 MΩ·cm at 25 °C.

Synthesis of PAm-*b*-PAA-*b*-POEGMEA THBC. Several compositions of poly(acrylamide)-*b*-poly(acrylic acid)-*b*-poly(oligo(ethylene glycol)-methyl ether acrylate) THBC with varying block masses were synthesized based on the same RAFT procedure in water. For the synthesis of a THBC with composition PAm_{144}-*b*-PAA_{52}-*b*-$POEGMEA_{29}$, for instance, BDMAT (0.26 g, $1{\cdot}10^{-3}$ mol), Am (10 g, $1.4{\cdot}10^{-1}$ mol), ACPA (0.026 g, $9{\cdot}10^{-5}$ mol), and water (34 mL) were mixed in a 250 mL Schlenk flask protected from light. The solution was purged with nitrogen at room temperature for 30 minutes, and then heated to 80 °C for 5 hours under stirring, ensuring polymerization of the PAm block. The obtained polymer was used as a macromolecular chain transfer agent for the polymerization of the second block. The solution was let to cool down to room temperature and AA (3.4 g, $5{\cdot}10^{-2}$ mol), ACPA (0.026 g, $9{\cdot}10^{-5}$ mol), and water (10.4 mL) were added to the reaction mixture. The solution was purged again with nitrogen at room temperature for 30 minutes, and then heated to 80 °C for 5 hours. This procedure was repeated to polymerize the third block, by adding OEGMEA (13.5 g, $3{\cdot}10^{-2}$ mol), ACPA (0.026 g, $9{\cdot}10^{-5}$ mol), and water (45 mL) to the reaction mixture. Following each block synthesis, a 1 mL aliquot was kept for ^{1}H NMR and elemental analysis. The resulting solution of PAm-*b*-PAA-*b*-POEGMEA, with a mass concentration of 23 wt%, was stored at 6 °C and used as such in subsequent steps. For the synthesis of other THBC compositions, the quantities of monomers were adapted to keep the mass concentration constant.

Synthesis of PAA-*b*-POEGMEA DHBC. Poly(acrylic acid)-*b*- poly(oligo(ethylene glycol)-methyl ether acrylate) DHBC was synthesized by aqueous RAFT polymerization following the procedure published by Phimphachanh *et al.*[30] CTPPA (0.26 g, $1{\cdot}10^{-3}$ mol), AA (3.6 g, $5{\cdot}10^{-2}$ mol), ACPA (0.028 g, $1{\cdot}10^{-4}$ mol), and water (9.2 mL) were mixed in a 250 mL Schlenk flask protected from light. The solution was purged with nitrogen at room temperature for 30 minutes and then heated to 80 °C for 5 hours. After cooling down to room temperature, the obtained PAA was used a macromolecular chain transfer agent for polymerization of the second block by adding OEGMEA (14.5 g, $3{\cdot}10^{-2}$ mol), ACPA (0.028 g, $1{\cdot}10^{-4}$ mol), and water (33 mL) to the mixture. The solution was purged again with nitrogen at room temperature for 30 minutes and then heated to 80 °C for 5 hours. Following each block synthesis, a 1 mL aliquot was kept for ^{1}H NMR analysis. The resulting solution of PAA-*b*-POEGMEA, with a mass concentration of 30 wt%, was stored at 6 °C and used as such.

Mesoporous silica material synthesis. For the synthesis of well-defined 0D silica nanostructures from PAm_{144}-*b*-PAA_{52}-*b*-$POEGMEA_{29}$ THBC, for instance, 32 mg of copolymer (corresponding to 141 mg of the 30 wt% stock solution) was dissolved with 14.5 mg of oligochitosan in 2.8 mL of water. The pH of the solution was raised to 4.5 by the addition of 10 µL of NH_4OH and the reaction mixture was left to stir for 30 minutes. Next, 45 µL of TMOS was added and the reaction was left under stirring overnight at room temperature. The obtained particles were precipitated at room temperature by adding 6 mL of dioxane and collected by centrifugation at 3600 g. Finally, the particles were redispersed in 3 mL water and stored at ambient temperature. For syntheses involving different polymers, including DHBC and other THBC compositions, the amounts of copolymers and oligochitosan were systematically adjusted to keep the EO molar concentration to 0.1 M, and the molar ratios N:AA and Si:EO to 1.

Characterization methods. The ^{1}H NMR analyses were performed at room temperature using D_2O as a solvent on a Bruker AVANCE III 600 MHz NMR Spectrometer. For these analyses, the copolymer was dried overnight at 80 °C, and about 10 mg of copolymer was then dissolved in 1 mL of D_2O. The C, H and N elemental analyses were performed using a ThermoFisher Scientific spectrometer iCE 3000. The polydispersity indices of the block copolymers were determined by SEC-MALS, using an AQUAGEL precolumn and two PL-AQUAGEL mixed H-column with phosphate buffer as the eluent at a flow rate of 1 mL/min. Unless specified, the TEM images were acquired using a Jeol JEM-1400 microscope operating at 100 kV and equipped with a 2048×2048 px Matataki Flash camera. For single particle reconstruction, TEM images were acquired using another Jeol JEM-1400 microscope, operating at 120 kV and equipped with a 4096×4096 px Gatan OneView camera. Unless specified, the TEM samples were prepared by dropping an aqueous suspension of the silica materials on TEM grids with a continuous carbon film and excess solution was blotted with a filter paper. Nitrogen sorption measurements were carried out at 77 K using a Tristar II Plus analyzer. Prior to measurements, the samples were calcined at 550 °C in air for 6 hours, and degassed at 10^{-3} Pa, 250 °C for 6 hours. Dynamic light scattering (DLS) measurements were performed using a Malvern Panalytical Advance Zetasizer Ultra with a detection at 173° to characterize the hydrodynamic diameter of 0D nanoparticles in water suspensions. SAXS measurements were performed at CoSAXS beamline (MAX IV synchrotron, Sweden), with a photon beam of energy 12.4 keV focusing on a scattering vector (q) range of 0.03-3 nm^{-1} and at SWING beamline (SOLEIL synchrotron, France) at an energy of 12 keV and a q range of 0.02-4 nm^{-1}. Sample solutions with an EO molar concentration of 0.1 M were placed in 1.5 mm quartz capillaries. The signals were corrected from transmission, and the solvent was measured for subtraction. Water was used for absolute scaling calibration.

ASSOCIATED CONTENT

The Supporting Information is available free of charge at [ACS website].

List of polymers with their respective block DP and number average molecular weight; ^{1}H NMR, SEC-MALS and elemental analyses of the polymer; Additional SAXS and TEM analyses of silica nanomaterials synthesized from different THBC compositions; UV absorption spectra of BDMAT, oligochitosan and of a mixture of THBC and $CuCl_2$.

ACKNOWLEDGEMENTS

A. V. thanks the University of Montpellier for funding. This work was partially funded by the Agence Nationale de la Recherche under grant number: ANR-21-CE08-0012-01. The authors thank Aurelien Lebrun for assistance with the ^{1}H NMR analyses, Philippe Gonzalez for the SEC-MALS analyses, Franck Godiard for the TEM analyses, Véronique Viguier for the TEM samples preparation, Magali Lefeuvre for elemental analysis, Antara Pal and Ann Terry for the SAXS analyses at MAX IV CoSAXS beamline (experiment number 20220490) and Javier Perez at SOLEIL SWING beamline (experiment number 20230807).

REFERENCES

(1) Vallet-Regí, M.; Schüth, F.; Lozano, D.; Colilla, M.; Manzano, M. Engineering Mesoporous Silica Nanoparticles for Drug Delivery: Where Are We after Two Decades? *Chem. Soc. Rev.* **2022**, *51* (13), 5365–5451.

(2) Croissant, J. G.; Fatieiev, Y.; Khashab, N. M. Degradability and Clearance of Silicon, Organosilica, Silsesquioxane, Silica Mixed Oxide, and Mesoporous Silica Nanoparticles. *Adv. Mater.* **2017**, *29* (9), 1604634.

(3) Janjua, T. I.; Cao, Y.; Yu, C.; Popat, A. Clinical Translation of Silica Nanoparticles. *Nat. Rev. Mater.* **2021**, *6* (12), 1072–1074.

(4) Talamini, L.; Picchetti, P.; Ferreira, L. M.; Sitia, G.; Russo, L.; Violatto, M. B.; Travaglini, L.; Fernandez Alarcon, J.; Righelli, L.; Bigini, P.; De Cola, L. Organosilica Cages Target Hepatic Sinusoidal Endothelial Cells Avoiding Macrophage Filtering. *ACS Nano* **2021**, *15* (6), 9701–9716.

(5) Noureddine, A.; Maestas-Olguin, A.; Tang, L.; Corman-Hijar, J. I.; Olewine, M.; Krawchuck, J. A.; Tsala Ebode, J.; Edeh, C.; Dang, C.; Negrete, O. A.; Watt, J.; Howard, T.; Coker, E. N.; Guo, J.; Brinker, C. J. Future of Mesoporous Silica Nanoparticles in Nanomedicine: Protocol for Reproducible Synthesis, Characterization, Lipid Coating, and Loading of Therapeutics (Chemotherapeutic, Proteins, siRNA and mRNA). *ACS Nano* **2023**, *17* (17), 16308–16325.

(6) Janjua, T. I.; Cao, Y.; Kleitz, F.; Linden, M.; Yu, C.; Popat, A. Silica Nanoparticles: A Review of Their Safety and Current Strategies to Overcome Biological Barriers. *Adv. Drug Deliv. Rev.* **2023**, *203*, 115115.

(7) Erstling, J. A.; Bag, N.; Gardinier, T. C.; Kohle, F. F. E.; DomNwachukwu, N.; Butler, S. D.; Kao, T.; Ma, K.; Turker, M. Z.; Feuer, G. B.; Lee, R.; Naguib, N.; Tallman, J. F.; Malarkey, H. F.; Tsaur, L.; Moore, W. L.; Chapman, D. V.; Aubert, T.; Mehta, S.; Cerione, R. A.; Weiss, R. S.; Baird, B. A.; Wiesner, U. B. Overcoming Barriers Associated with Oral Delivery of Differently Sized Fluorescent Core-Shell Silica Nanoparticles. *Adv. Mater.* **2024**, *36* (1), 2305937.

(8) Li, J.; Liu, X.; Ma, K.; Liu, Y.; Meng, H. Understanding of Surface Chemistry of Silica-Based Nanomaterials Contributes to the Design of Safe and Efficacious Nanomedicine. *Matter.* **2023**, *6* (8), 2564–2567.

(9) Zhao, T.; Elzatahry, A.; Li, X.; Zhao, D. Single-Micelle-Directed Synthesis of Mesoporous Materials. *Nat. Rev. Mater.* **2019**, *4* (12), 775–791.

(10) Qiu, P.; Yang, J.; Jiang, W.; Wang, L.; Fan, Y.; Luo, W. Interfacial Engineering of Core-Shell Structured Mesoporous Architectures from Single-Micelle Building Blocks. *Nano Today* **2020**, *35*, 100940.

(11) Aubert, T.; Ma, K.; Tan, K. W.; Wiesner, U. Two-Dimensional Superstructures of Silica Cages. *Adv. Mater.* **2020**, *32* (21), 1908362.

(12) Ma, K.; Gong, Y.; Aubert, T.; Turker, M. Z.; Kao, T.; Doerschuk, P. C.; Wiesner, U. Self-Assembly of Highly Symmetrical, Ultrasmall Inorganic Cages Directed by Surfactant Micelles. *Nature* **2018**, *558* (7711), 577–580.

(13) Li, X.; Iocozzia, J.; Chen, Y.; Zhao, S.; Cui, X.; Wang, W.; Yu, H.; Lin, S.; Lin, Z. From Precision Synthesis of Block Copolymers to Properties and Applications of Nanoparticles. *Angew. Chem. Int. Ed.* **2018**, *57* (8), 2046–2070.

(14) Kim, K.-W.; Park, B.; Kim, J.; Jo, C.; Kim, J. K. Recent Progress in Block Copolymer Soft-Template-Assisted Synthesis of Versatile Mesoporous Materials for Energy Storage Systems. *J. Mater. Chem. A* **2023**, *11* (14), 7358–7386.

(15) Yu, F.; Wiesner, U. The Emerging Field of Block Copolymer Self-Assembly-Directed Quantum Materials. *Polymer* **2023**, *281*, 126063.

(16) Baccile, N.; Reboul, J.; Blanc, B.; Coq, B.; Lacroix-Desmazes, P.; In, M.; Gérardin, C. Ecodesign of Ordered Mesoporous Materials Obtained with Switchable Micellar Assemblies. *Angew. Chem. Int. Ed.* **2008**, *47* (44), 8433–8437.

(17) Bathfield, M.; Warnant, J.; Gérardin, C.; Lacroix-Desmazes, P. Asymmetric Neutral, Cationic and Anionic PEO-Based Double-Hydrophilic Block Copolymers (DHBCs): Synthesis and Reversible Micellization Triggered by Temperature or pH. *Polym. Chem.* **2015**, *6* (8), 1339–1349.
(18) Molina, E.; Mathonnat, M.; Richard, J.; Lacroix-Desmazes, P.; In, M.; Dieudonné, P.; Cacciaguerra, T.; Gérardin, C.; Marcotte, N. pH-Mediated Control over the Mesostructure of Ordered Mesoporous Materials Templated by Polyion Complex Micelles. *Beilstein J. Nanotechnol.* **2019**, *10*, 144–156.
(19) El Jundi, A.; Buwalda, S. J.; Bakkour, Y.; Garric, X.; Nottelet, B. Double Hydrophilic Block Copolymers Self-Assemblies in Biomedical Applications. *Adv. Colloid Interface Sci.* **2020**, *283*, 102213.
(20) Sing, C. E.; Perry, S. L. Recent Progress in the Science of Complex Coacervation. *Soft Matter* **2020**, *16* (12), 2885–2914.
(21) Richard, J.; Phimphachanh, A.; Schneider, J.; Nandi, S.; Laurent, E.; Lacroix-Desmazes, P.; Trens, P.; Devautour-Vinot, S.; Marcotte, N.; Gérardin, C. Integrated Process for Structuring and Functionalizing Ordered Mesoporous Silica to Achieve Superprotonic Conductivity. *Chem. Mater.* **2022**, *34* (17), 7828–7836.
(22) Birault, A.; Molina, E.; Toquer, G.; Lacroix-Desmazes, P.; Marcotte, N.; Carcel, C.; Katouli, M.; Bartlett, J. R.; Gérardin, C.; Wong Chi Man, M. Large-Pore Periodic Mesoporous Organosilicas as Advanced Bactericide Platforms. *ACS Appl. Bio Mater.* **2018**, *1* (6), 1787–1792.
(23) Birault, A.; Molina, E.; Carcel, C.; Bartlett, J.; Marcotte, N.; Toquer, G.; Lacroix-Desmazes, P.; Gerardin, C.; Wong Chi Man, M. Synthesis of Lamellar Mesostructured Phenylene-Bridged Periodic Mesoporous Organosilicas (PMO) Templated by Polyion Complex (PIC) Micelles. *J. Sol-Gel Sci. Technol.* **2019**, *89*, 189–195.
(24) Houssein, D.; Warnant, J.; Molina, E.; Cacciaguerra, T.; Gérardin, C.; Marcotte, N. Mesoporous Silica Templated by Polyion Complex Micelles: A Versatile Approach for Controlling the Mesostructure. *Micropor. Mesopor. Mat.* **2017**, *239*, 244–252.
(25) Richard, J.; Phimphachanh, A.; Jamet-Fournier, A.; Cacciaguerra, T.; Dieudonné-George, P.; Cot, D.; Destarac, M.; Lacroix-Desmazes, P.; In, M.; Marcotte, N.; Gérardin, C. Dual Control of External Surface and Internal Pore Structure of Small Ordered Mesoporous Silica Particles Directed by Mixed Polyion Complex Micelles. *Micropor. Mesopor. Mat.* **2022**, *338*, 111915.
(26) Sohn, H.; Shin, H.-W.; Lee, S.-M. Metal-Mediated Morphology Regulation of Self-Assembled Double-Hydrophilic Block Copolymers. *ACS Macro Lett.* **2020**, *9* (4), 600–605.
(27) Boudier, A.; Aubert-Pouëssel, A.; Gérardin, C.; Devoisselle, J.-M.; Bégu, S.; Louis-Plence, P.; Quentin, J.; Jorgensen, C. Tripartite siRNA Micelles as Controlled Delivery Systems for Primary Dendritic Cells. *Drug Dev. Ind. Pharm.* **2009**, *35* (8), 950–958.
(28) Molina, E.; Warnant, J.; Mathonnat, M.; Bathfield, M.; In, M.; Laurencin, D.; Jérôme, C.; Lacroix-Desmazes, P.; Marcotte, N.; Gérardin, C. Drug–Polymer Electrostatic Complexes as New Structuring Agents for the Formation of Drug-Loaded Ordered Mesoporous Silica. *Langmuir* **2015**, *31* (47), 12839–12844.
(29) Reboul, J.; Nugay, T.; Anik, N.; Cottet, H.; Ponsinet, V.; In, M.; Lacroix-Desmazes, P.; Gérardin, C. Synthesis of Double Hydrophilic Block Copolymers and Induced Assembly with Oligochitosan for the Preparation of Polyion Complex Micelles. *Soft Matter* **2011**, *7* (12), 5836.
(30) Phimphachanh, A.; Chamieh, J.; Leclercq, L.; Harrisson, S.; Destarac, M.; Lacroix-Desmazes, P.; Gérardin, C.; In, M.; Cottet, H. Characterization of Diblock Copolymers by Capillary Electrophoresis: From Electrophoretic Mobility Distribution to Distribution of Composition. *Macromolecules* **2020**, *53* (1), 334–345.
(31) Guinier, A.; Fournet, G.; Walker, C. B.; Vineyard, G. H. Small-Angle Scattering of X-Rays. *Phys. Today* **1956**, *9* (8), 38–39.
(32) Gérardin, C.; Reboul, J.; Bonne, M.; Lebeau, B. Ecodesign of Ordered Mesoporous Silica Materials. *Chem. Soc. Rev.* **2013**, *42* (9), 4217.

(33) Tang, G.; Peng, L.; Baldwin, P. R.; Mann, D. S.; Jiang, W.; Rees, I.; Ludtke, S. J. EMAN2: An Extensible Image Processing Suite for Electron Microscopy. *J. Struct. Biol.* **2007**, *157* (1), 38–46.
(34) Bell, J. M.; Chen, M.; Durmaz, T.; Fluty, A. C.; Ludtke, S. J. New Software Tools in EMAN2 Inspired by EMDatabank Map Challenge. *J. Struct. Biol.* **2018**, *204* (2), 283–290.
(35) Bell, J. M.; Chen, M.; Baldwin, P. R.; Ludtke, S. J. High Resolution Single Particle Refinement in EMAN2.1. *Methods* **2016**, *100*, 25–34.
(36) Xiao, C.; Fujita, N.; Miyasaka, K.; Sakamoto, Y.; Terasaki, O. Dodecagonal Tiling in Mesoporous Silica. *Nature* **2012**, *487* (7407), 349–353.
(37) Pettersen, E. F.; Goddard, T. D.; Huang, C. C.; Couch, G. S.; Greenblatt, D. M.; Meng, E. C.; Ferrin, T. E. UCSF Chimera—A Visualization System for Exploratory Research and Analysis. *J. Comput. Chem.* **2004**, *25* (13), 1605–1612.
(38) Iatridi, Z.; Bokias, G.; Kallitsis, J. K. Physicochemical Study of the Complexation of Poly(Acrylic Acid) with Cu^{2+} Ions in Water. *J. Appl. Polym. Sci.* **2008**, *108* (2), 769–776.
(39) Nishiyama, N.; Yokoyama, M.; Aoyagi, T.; Okano, T.; Sakurai, Y.; Kataoka, K. Preparation and Characterization of Self-Assembled Polymer−Metal Complex Micelle from *Cis* -Dichlorodiammineplatinum(II) and Poly(Ethylene Glycol)−Poly(α,β-Aspartic Acid) Block Copolymer in an Aqueous Medium. *Langmuir* **1999**, *15* (2), 377–383.
(40) Gineste, S.; Mingotaud, C. Double-Hydrophilic Block Copolymer–Metal Ion Associations: Structures, Properties and Applications. *Adv. Colloid Interface Sci.* **2023**, *311*, 102808.
(41) Sanson, N.; Bouyer, F.; Destarac, M.; In, M.; Gérardin, C. Hybrid Polyion Complex Micelles Formed from Double Hydrophilic Block Copolymers and Multivalent Metal Ions: Size Control and Nanostructure. *Langmuir* **2012**, *28* (8), 3773–3782.
(42) Layrac, G.; Gérardin, C.; Tichit, D.; Harrisson, S.; Destarac, M. Hybrid Polyion Complex Micelles from Poly(Vinylphosphonic Acid)-Based Double Hydrophilic Block Copolymers and Divalent Transition Metal Ions. *Polym. J.* **2015**, *72*, 292–300.
(43) Lowe, A. B.; McCormick, C. L. Reversible Addition–Fragmentation Chain Transfer (RAFT) Radical Polymerization and the Synthesis of Water-Soluble (Co)Polymers under Homogeneous Conditions in Organic and Aqueous Media. *Prog. Polym. Sci.* **2007**, *32* (3), 283–351.
(44) Bray, C.; Peltier, R.; Kim, H.; Mastrangelo, A.; Perrier, S. Anionic Multiblock Core Cross-Linked Star Copolymers via RAFT Polymerization. *Polym. Chem.* **2017**, *8* (36), 5513–5524.

For Table of Contents Only